Journal of Magnetic Resonance 197 (2009) 14–19

Contents lists available at ScienceDirect

Journal of Magnetic Resonance

journal homepage: www.elsevier.com/locate/jmr

Supercycled homonuclear dipolar decoupling sequences in solid-state NMR

Subhradip Paul [a], Rajendra Singh Thakur [a], Mithun Goswami [a], Andrea C. Sauerwein [b], Salvatore Mamone [b], Maria Concistrè [b], Hans Förster [c], Malcolm H. Levitt [b], P.K. Madhu [a,*]

[a] Department of Chemical Sciences, Tata Institute of Fundamental Research, Homi Bhabha Road, Colaba, Mumbai 400 005, India
[b] Department of Chemistry, University of Southampton, Southampton SO17 1BJ, UK
[c] Solids NMR Applications, Bruker Biospin GmbH, Silberstreifen 4, Rheinstetten 76287, Germany

ARTICLE INFO

Article history:
Received 1 September 2008
Revised 7 November 2008
Available online 27 November 2008

Keywords:
Solid-state NMR
Homonuclear dipolar decoupling
PMLG
DUMBO
MAS
^{1}H spectra

ABSTRACT

We compare the performance of the windowed phase-modulated Lee–Goldburg (*w*PMLG) and the windowed decoupling using mind boggling optimisation (*w*DUMBO) sequences at various magic-angle spinning rates and nutation frequencies of the pulses. Additionally, we introduce a supercycled version of *w*DUMBO and compare its efficiency with that of the non-supercycled implementation of *w*DUMBO. The efficiency of the supercycled version of *w*PMLG, denoted *w*PMLG-S2, is compared with a new supercycled version of *w*PMLG that we notate as *w*PMLG-S3. The interaction between the supercycled homonuclear dipolar decoupling sequences and the sample rotation is analysed using symmetry-based selection rules.

1. Introduction

High-resolution proton nuclear magnetic resonance (NMR) spectroscopy is possible in the solid-state, due to the development of combined magic-angle spinning and multiple-pulse techniques, that average out the strong homonuclear dipolar couplings [1,2]. Among the various multiple-pulse schemes that are normally employed, those that have been shown to perform well at MAS frequencies of 10–25 kHz are the frequency-switched Lee–Goldburg (FSLG) [3,4], the phase-modulated Lee–Goldburg (PMLG) [5,6], and the decoupling using mind boggling optimisation (DUMBO) [7] sequences. FSLG and PMLG are the sequences of choice in most two-dimensional (2D) experiments requiring high-resolution ^{1}H spectra, for example, in 2D heterocorrelation spectroscopy [8–12] and 2D double quantum–single quantum correlation spectroscopy [13]. Both double-quantum and triple-quantum ^{1}H spectroscopy have also been reported with the use of DUMBO [14–16]. *w*PMLG has been widely used to obtain high-resolution ^{1}H spectra in one-dimensional (1D) experiments. A detailed report on the various experimental aspects, such as optimisation protocols of FSLG, PMLG, and *w*PMLG, has recently been published [17].

The windowed 1D version of PMLG, the *w*PMLG sequence [18], has evolved in last 10 years in its experimental implementation and theoretical understanding, which is based on bimodal Floquet theory [2]. A supercycled version of the *w*PMLG scheme was recently implemented, notated as $w\text{PMLG}^{xx}_{\text{mm}}$ [19,20]. This supercycled version of *w*PMLG generates an effective *z*-rotation for the transverse magnetisation, resulting in good spectra at a wider range of resonance offsets, a more robust scaling factor, and relatively good performance at moderately high MAS frequencies. However, the realisation of this experiment at high MAS frequencies such as 25–30 kHz requires high RF power (nutation frequencies around 150–180 kHz) as discussed below.

In this article the notation *w*PMLG5-S(P) refers to a supercycle constructed by *P* *w*PMLG5 elements with overall phases incremented by $2\pi/P$. A single *w*PMLG5 element consists of 10 pulses followed by an observation window, where the pulse phases and timings are specified explicitly in Refs. [2,20]. The sequence denoted as $w\text{PMLG}^{xx}_{\text{mm}}$ in Refs. [19,20] is henceforth referred to as *w*PMLG-S2.

The 1D version of the DUMBO scheme with windows (*w*DUMBO) has also been shown to work well up to a MAS frequency of ca. 25 kHz [21]. A detailed theoretical study of *w*DUMBO has never been attempted, although most of the modifications suggested to improve the *w*PMLG scheme can be extended to *w*DUMBO without any loss of generality.

Here we introduce a supercycled version of *w*DUMBO, denoted *w*DUMBO-S2, which uses a supercycling scheme similar to *w*PMLG-S2, to enable its implementation at high MAS frequencies of 30 kHz. We compare the performance of *w*DUMBO and *w*DUMBO-S2, *w*PMLG-S2, and *w*DUMBO-S2 at various spinning frequencies. The performance of *w*PMLG-S2 is then compared with another supercycled version of *w*PMLG called *w*PMLG-S3 which

* Corresponding author. Fax: +91 22 2280 4610.
E-mail address: madhu@tifr.res.in (P.K. Madhu).

1090-7807/$ - see front matter © 2008 Elsevier Inc. All rights reserved.
doi:10.1016/j.jmr.2008.11.011

allows the implementation of *w*PMLG in regimes where *w*PMLG-S2 is not very effective. We use a symmetry-based average Hamiltonian analysis to predict the conditions under which particular supercycles are most appropriate.

2. Experimental

The experiments comparing *w*DUMBO and *w*DUMBO-S2, and *w*PMLG5-S2 and *w*DUMBO-S2 (Figs. 2–4) were performed on a sample of glycine in a Bruker AVIII 700 MHz spectrometer with a narrow-bore magnet (bore size 54 mm) using a 2.5 mm double-resonance probe. All the other experiments on glycine (Figs. 5 and 7) and L-histidine · HCl · H_2O (Fig. 6) were performed on a Bruker AVI 500 MHz spectrometer with a wide-bore magnet (bore size 89 mm) using a 4 mm triple-resonance probe. In all cases the rotor was completely filled with the sample. The scaling factors were determined by comparing the spectrum of glycine, obtained with a homonuclear dipolar decoupling scheme, with that in the solution state. The chemical shifts in the glycine spectra were referenced by assigning the midpoint of the two methylene proton peaks of glycine to 3.52 ppm, which corresponds to the methylene proton chemical shift of glycine in solution state [22].

3. Methods

The pulse sequences implemented in this article are depicted in Fig. 1. Fig. 1a illustrates a supercycled homonuclear dipolar decoupling sequence with $P = 2$ in which A can either be the PMLG or the DUMBO scheme. Each *w*PMLG or *w*DUMBO block (consisting of a single homonuclear decoupling sequence followed by an observation window) is considered to be a cyclic element with total duration denoted τ_C. A data point (denoted by the asterisk) is acquired during each acquisition window. The basic pulse sequence block, A, consists of 10 pulses for PMLG5 [18] and 64 pulses for DUMBO [7], with their phases shown in Fig. 1a. Supercycling is implemented for both *w*PMLG-S2 and *w*DUMBO-S2 by incrementing the phases of consecutive pulse sequence blocks by 180°. Fig. 1b shows the *w*PMLG-S3 sequence which is constructed by incrementing the overall phase of the *w*PMLG blocks in steps of 120°.

4. Results and discussion

Fig. 2 compares the performance of the *w*DUMBO-S2 scheme and the non-supercycled version of *w*DUMBO for a sample of glycine at MAS frequencies of 10 kHz and 25 kHz. The quality of the spectrum improves with supercycling of *w*DUMBO especially at the higher MAS frequency of 25 kHz as reported for *w*PMLG-S2 [19]. The supercycling in *w*DUMBO-S2 removes the criterion of off-resonant irradiation, which is normally required for homonuclear decoupling under the DUMBO scheme. The effective *z*-rotation of the spins allows *w*DUMBO-S2 to perform better at high spinning frequencies of up to 30 kHz which was attempted here. In general, the experimental properties of the *w*DUMBO-S2 sequence are similar to those of *w*PMLG-S2.

A comparison of the performance of the *w*PMLG5-S2 and the *w*DUMBO-S2 schemes is shown in Figs. 3 and 4 at MAS frequencies of 10 kHz, 20 kHz, and 30 kHz. Fig. 3 shows the raw spectra whilst Fig. 4 shows spectra with adjusted horizontal scales taking into account the scaling factor for the isotropic chemical shifts. Our results show that high-resolution proton spectra can be obtained with both the *w*PMLG and the *w*DUMBO schemes using supercycled versions up to MAS frequencies of 30 kHz. It is possible that these schemes will result in high-resolution proton spectra at MAS frequencies higher than 30 kHz. Fig. 3 shows that the raw line width obtained with *w*DUMBO-S2 is smaller than that obtained with *w*PMLG5-S2. The scaling factor of both *w*PMLG5-S2 and *w*DUMBO-S2 decreases at high MAS frequencies which is primarily due to the requirement of stronger RF pulses [2].

It is clear from Figs. 3 and 4 that the RF field strength required for optimal performance increases with MAS frequencies for both the *w*PMLG5-S2 and the *w*DUMBO-S2 sequences. At any MAS frequency *w*DUMBO-S2 requires higher RF fields than *w*PMLG5-S2. This becomes significant at the MAS frequency of 30 kHz with *w*DUMBO-S2 requiring 250 kHz of RF field strength compared to 180 kHz required for *w*PMLG5-S2. In addition, both sequences suffer from the influence of rotary-resonance lines [2]. The presence of these lines close to a real resonance can broaden it. However, the positions of the rotary resonances can be predicted based on the cycle frequency of the scheme and the MAS frequency, thereby

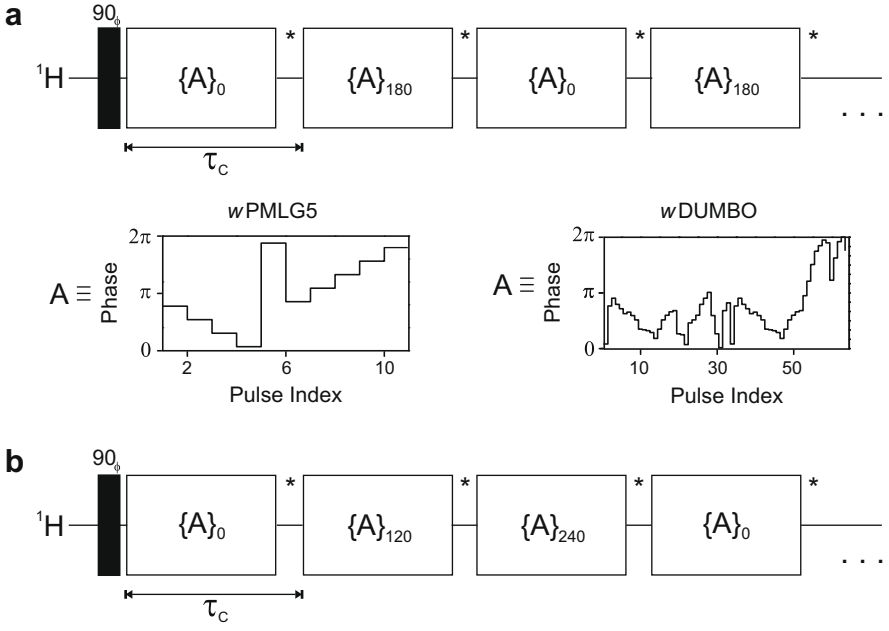

Fig. 1. The schematic of (a) *w*PMLG-S2, *w*DUMBO-S2, and (b) *w*PMLG-S3 pulse schemes with A depicting the phase profile of either *w*PMLG5 or *w*DUMBO. τ_C denotes the duration of the homonuclear dipolar decoupling pulse element including the observation window.

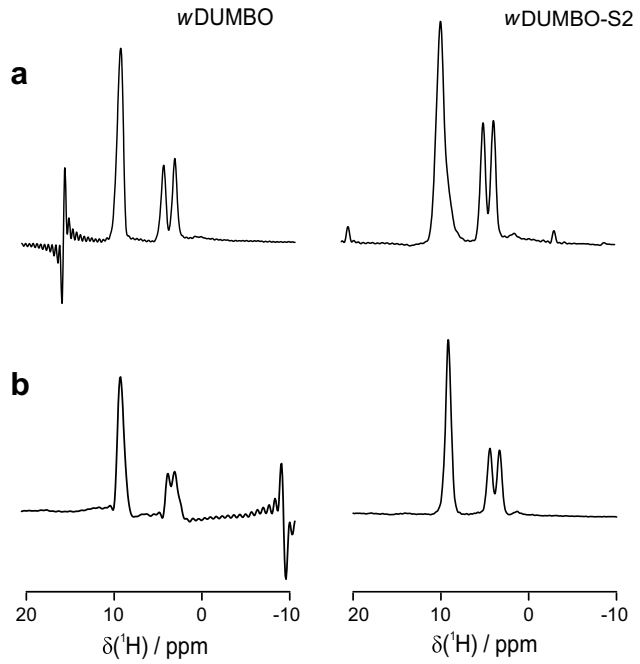

Fig. 2. The scaled ^{1}H spectra of glycine with *w*DUMBO (left column) and *w*DUMBO-S2 (right column) acquired with (a) MAS frequency of 10 kHz and RF field strength of 104 kHz, and (b) MAS frequency of 25 kHz and RF field strength of 208 kHz. One DUMBO element was of duration 24 μs. The observation window was 4 μs. The off-resonance values at which the spectra were acquired are +8 kHz for *w*DUMBO at MAS frequency of 10 kHz, 0 kHz for *w*DUMBO at spinning frequency 25 kHz, +4 kHz for *w*DUMBO-S2 at both 10 kHz and 25 kHz of MAS frequency. The spectral frequency axis was scaled by a factor of 0.6 in (a) and 0.19 in (b) for *w*DUMBO and 0.38 in (a) and 0.21 in (b) for *w*DUMBO-S2. The experiments were done on a Bruker AVIII 700 MHz spectrometer using a 2.5 mm double-resonance probe.

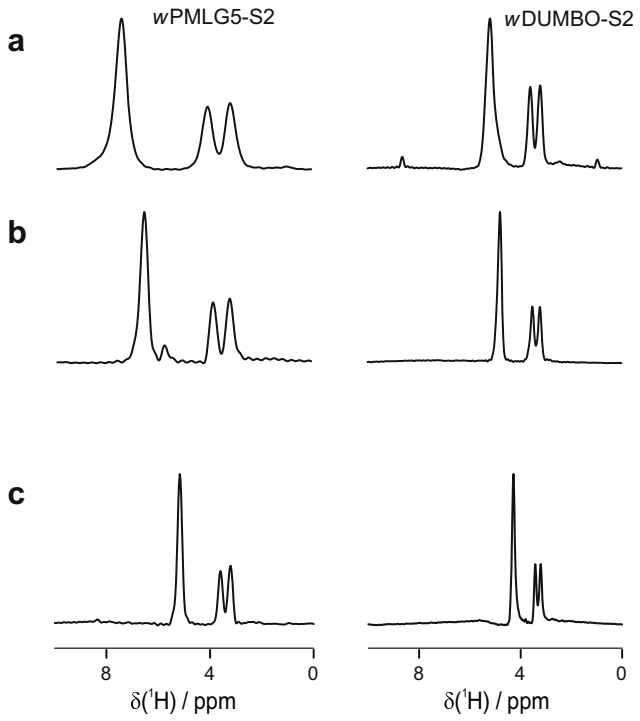

Fig. 3. The raw ^{1}H spectra of glycine with *w*PMLG5-S2 (left column) and *w*DUMBO-S2 (right column) acquired with MAS frequency of (a) 10 kHz, (b) 20 kHz, and (c) 30 kHz. The RF field strengths for *w*PMLG5-S2 and *w*DUMBO-S2 were, respectively, 100 kHz and 104 kHz in (a), 140 kHz and 156 kHz in (b), and 180 kHz and 250 kHz in (c). The duration of one PMLG5 element was 16.33 μs in (a), 11.67 μs in (b), and 9.07 μs in (c). The duration of one DUMBO element was 24 μs in (a), 16 μs in (b), and 10 μs in (c). The observation window was 4 μs. The experiments were done on a Bruker AVIII 700 MHz spectrometer using a 2.5 mm double-resonance probe.

avoiding the occurrence of these over a spectral window where the real resonances occur [2]. There is a sufficient spectral window range of 8–10 kHz free of rotary-resonance lines which allows easy execution of both sequences in any sample. The near effective *z*-rotation clearly helps both schemes in achieving such a spectral window. Our data seems to indicate that the *w*PMLG5 scheme will be difficult to implement at spinning frequencies higher than 30 kHz, since the ratio of the cycle frequency of the *w*PMLG5 scheme (taking into account the pulse duration and the observation window delay) to the MAS frequency, ω_c/ω_r should be at least 2.5 [2]. It is possible to envisage applications of the *w*PMLG5 schemes at high MAS rates for lower values of ω_c/ω_r. This will, however, require shorter pulse durations and higher RF field strengths.

In most cases, the experimental performance of the *w*PMLG sequence improves when the supercycled version *w*PMLG-S2 is used. However, the supercycled version still fails at certain ratios of cycle frequency and spinning frequency due to the destructive interference between the RF field and the MAS, as discussed below. This problem can be overcome by using a different supercycled version of *w*PMLG, in which the overall phase of a *w*PMLG unit is varied as 0°, 120°, and 240°. This scheme, notated as *w*PMLG-S3, provides a complementary performance to that of *w*PMLG-S2. Its phase cycle was adapted from the MSHOT-3 sequence [23,24].

Fig. 5 shows proton spectra of glycine obtained with *w*PMLG5-S2 (left column) and *w*PMLG5-S3 (right column) schemes at spinning frequencies of 14 kHz and 10 kHz, respectively, for a wide range of off-resonance irradiation frequencies from +8 kHz to 0 kHz in steps of 2 kHz at an RF field strength of 85 kHz. Keeping other experimental conditions the same, the spectrum obtained with *w*PMLG5-S2 at the MAS frequency of 10 kHz and that

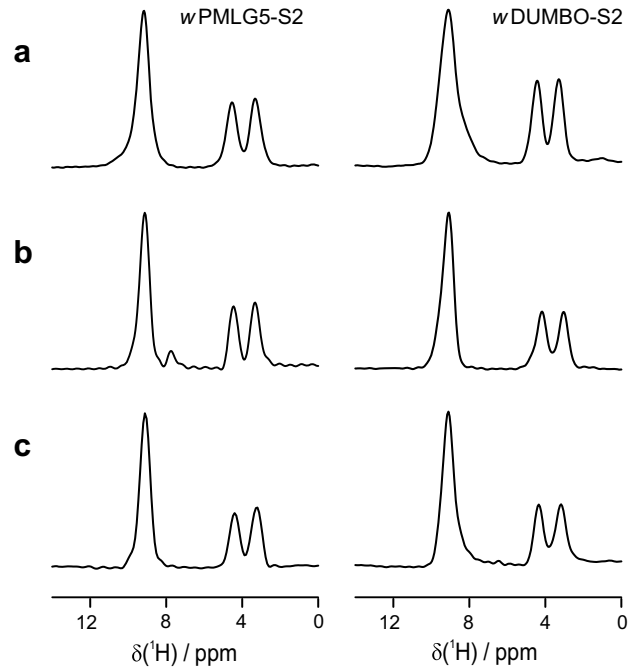

Fig. 4. ^{1}H spectra of glycine with *w*PMLG5-S2 (left column) and *w*DUMBO-S2 (right column) with horizontal scales adjusted taking into account the scaling factor for the isotropic chemical shifts. The empirically derived scaling factors in case of *w*PMLG5-S2 are (a) 0.73, (b) 0.57, and (c) 0.33 and those for *w*DUMBO-S2 are (a) 0.33, (b) 0.26, and (c) 0.18. All other details are the same as in Fig. 3. The experiments were done on a Bruker AVIII 700 MHz spectrometer using a 2.5 mm double-resonance probe.

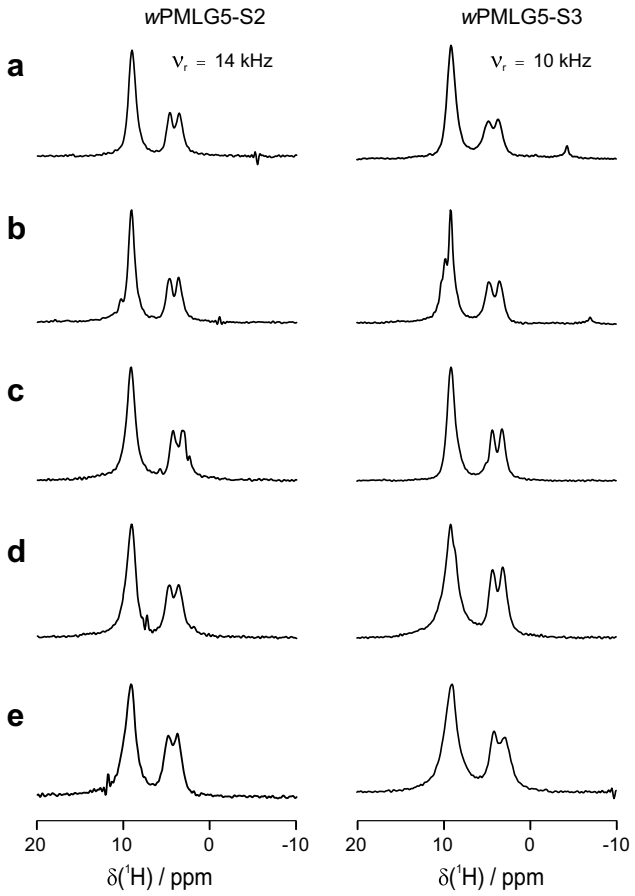

Fig. 5. The scaled ^{1}H spectrum of glycine obtained with the *w*PMLG5-S2 (left column) scheme at a MAS frequency of 14 kHz and *w*PMLG5-S3 (right column) scheme at a MAS frequency of 14 kHz. The off-resonance irradiation frequency was (a) 8 kHz, (b) 6 kHz, (c) 4 kHz, (d) 2 kHz, and (e) 0 kHz. The RF field strength was 85 kHz. The duration of one PMLG5 element was 18.5 μs and the observation window was 5.8 μs. The spectral frequency axis was scaled by a factor of 0.44 for *w*PMLG5-S2 and 0.46 for *w*PMLG5-S3. The experiments were done on a Bruker AVI 500 MHz spectrometer using a 4 mm triple-resonance probe.

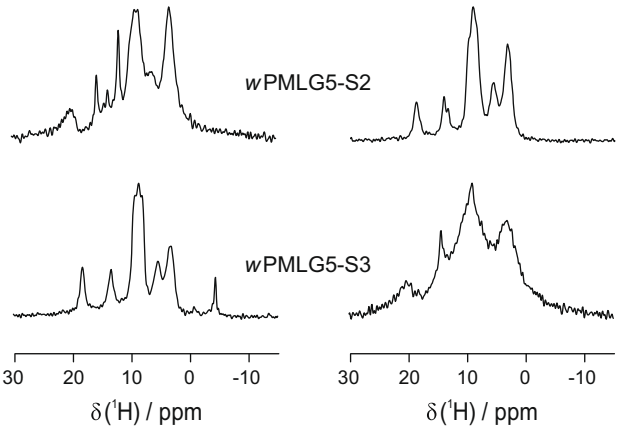

Fig. 6. The scaled ^{1}H spectrum of L-histidine · HCl · H_2O obtained with *w*PMLG5-S2 (top trace) and *w*PMLG5-S3 (bottom trace) at a MAS frequency of 10 kHz (left column) and 14 kHz (right column). The duration of one PMLG5 element was 18.5 μs and the observation window was 5.8 μs. The off-resonance irradiation frequency was 7 kHz. The RF field strength was 85 kHz. The spectral frequency axis was scaled by a factor of 0.44 for *w*PMLG5-S2 and 0.46 for *w*PMLG5-S3. The experiments were done on a Bruker AVI 500 MHz spectrometer using a 4 mm triple-resonance probe.

obtained with *w*PMLG5-S3 at the MAS frequency of 14 kHz was of inferior quality (data not shown). Hence, although for a given set of experimental conditions, *w*PMLG5-S2 fails at the MAS frequency of 10 kHz, *w*PMLG5-S3 yields good spectra and vice versa at the MAS frequency of 14 kHz.

Fig. 6 substantiates the above observation on a sample of L-histidine · HCl · H_2O. The upper spectra were acquired with *w*PMLG5-S2, whilst the lower spectra were acquired with *w*PMLG5-S3. The spectra in the left and right columns were obtained at spinning frequencies of 10 kHz and 14 kHz, respectively. As in the case of glycine *w*PMLG5-S2 performs well at the MAS frequency of 14 kHz whilst *w*PMLG5-S3 performs well at the MAS frequency of 10 kHz.

A systematic study of the performance of the *w*PMLG5-S2 and the *w*PMLG5-S3 sequences was carried out by monitoring the peak height of the NH_3^+ peak of glycine as a function of the off-resonance irradiation frequency and MAS frequency. The results of this study are shown in Fig. 7 at an RF field strength of 85 kHz which shows that the two supercycled versions of PMLG have a complementary performance profile.

The interaction of supercycled homonuclear decoupling sequences with the magic-angle sample rotation may be analysed by a variety of theoretical methods, including bimodal Floquet theory [2] and average Hamiltonian theory [25]. The approach followed here is to seek an analogy between homonuclear decoupling sequences in rotating samples and symmetry-based recoupling sequences [26–30], in particular those of the class CN_n^ν. For example, consider a supercycled *w*PMLG sequence in which the overall phases of consecutive *w*PMLG sequences are incremented in steps of $2\pi/P$, where P is an integer. One PMLG block followed by an observation window may be regarded as the basic cycle element of a symmetry-based sequence. The total duration of the C-element is denoted τ_C. Consider the case in which N C-elements occupy exactly n rotational periods, where N and n are both integers, i.e. $N\tau_C = n\tau_r$, where a rotor period is given by $\tau_r = 2\pi/\omega_r$, and ω_r is the spinning frequency. In this case the supercycled *w*PMLG sequence conforms to the symmetry $C(NP)_{nP}^N$. The results in Refs. [26–30] may be applied to derive the following selection rule for the symmetry-allowed first-order average Hamiltonian terms

$$\overline{\mathcal{H}}^{(1)}_{lm\lambda\mu} = 0 \quad \text{if} \quad (mnP - \mu N) \neq KNP \tag{1}$$

where K is an integer. Here $lm\lambda\mu$ denotes the space and spin quantum numbers of a spin interaction component. As described in Ref. [29], homonuclear dipole–dipole interactions are described by ranks $l = \lambda = 2$, whilst for the chemical shift anisotropy, $l = 2$ and $\lambda = 1$. Components with $(l, m) = (2, 0)$ vanish for exact magic-angle spinning.

It is easily shown from Eq. (1) that the condition $N = n$ leads to many symmetry-allowed first-order average Hamiltonian terms and hence poor homonuclear decoupling. In this case, the left-hand side of the inequality in Eq. (1) takes the form $m \neq K$ for components with $\mu = 0$. The inequality may be broken by choosing $K = m$ and hence all terms of the form $\overline{\mathcal{H}}^{(1)}_{lm\lambda 0}$ are symmetry-allowed in this case. The condition $N = 2n$ also leads to poor homonuclear decoupling. In this case, the left-hand side of the inequality in Eq. (1) takes the form $m \neq 2K$ for components with $\mu = 0$. This may be broken for the $m = \pm 2$ components of the dipole–dipole interaction by choosing $K = \pm 1$. The condition $N = 2n$ therefore leads to symmetry-allowed dipole–dipole coupling terms of the form $\overline{\mathcal{H}}^{(1)}_{2\pm 220}$, irrespective of the supercycle order. Conditions under which one or two *w*PMLG elements fit into a single rotor period should therefore always be avoided, if good homonuclear decoupling is desired. Recoupling is also encountered at all conditions $P = N/n$ and $2P = N/n$. In the first case, terms with $m = \mu$ are

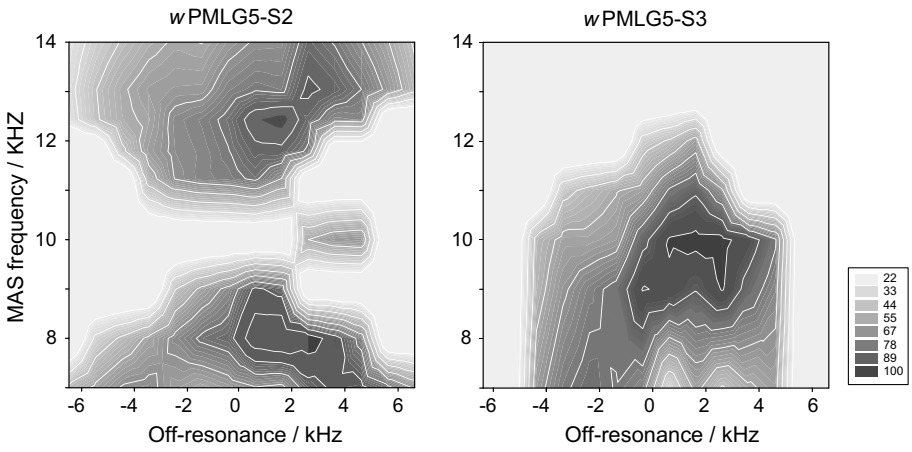

Fig. 7. Contour plots depicting the peak height of the NH_3^+ resonance of glycine as a function of the off-resonance irradiation frequency and MAS frequency for an RF field strength of 85 kHz obtained with the *w*PMLG5-S2 scheme and the *w*PMLG5-S3 scheme. The duration of one PMLG5 element was 18.5 μs and the observation window was 5.8 μs. The peak heights are normalised with respect to the one obtained with the best decoupling conditions the peak height of which is marked as 100. The experiments were done on a Bruker AVI 500 MHz spectrometer using a 4 mm triple-resonance probe.

recoupled. In the second case, terms with $m = 2\mu$ are recoupled. This implies that for the best decoupling, neither one nor two complete supercycles should fit into one rotor period.

The result of a general symmetry analysis of supercycled rotor-synchronised homonuclear decoupling sequences is shown in Fig. 8. The depth of shading indicates the total number of symmetry-allowed first-order dipole–dipole and chemical shift anisotropy terms, obtained from a numerical analysis of the selection rule in Eq. (1). White regions in the plot correspond to conditions under which good homonuclear decoupling is anticipated, whilst the dark bands indicate conditions that should be avoided. The left-hand axis indicates the number of *w*PMLG elements per rotor period, whilst the horizontal axis indicates the supercycle order *P*. The left-hand edge of the plot corresponds to $P = 1$ (no supercycling). The supercycles discussed in this paper correspond to $P = 2$ and $P = 3$. The right-hand label indicates the spinning frequency for the specific case of a C-element duration of τ_C = 24.3 μs, which corresponds to the experimental parameters used in Figs. 5–7.

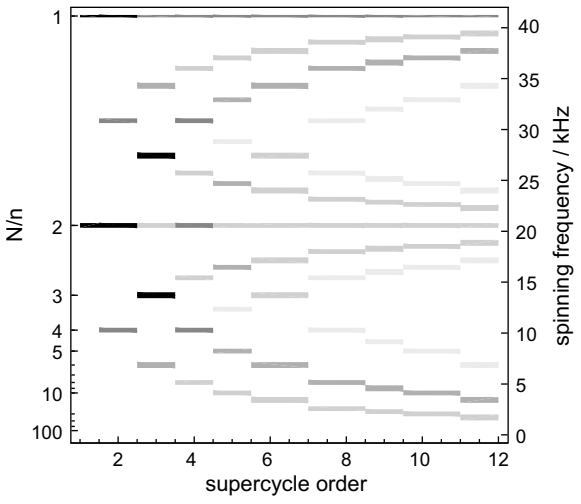

Fig. 8. Symmetry-based average Hamiltonian analysis of first-order recoupling conditions for rotor-synchronised homonuclear dipolar decoupling supercycles. The depth of the shading in the horizontal bars is proportional to the number of symmetry-allowed dipole–dipole and chemical shift anisotropy terms. Horizontal axis: The supercycle order *P*. Left-hand vertical axis: the number of decoupling cycles per rotor period. The right-hand axis shows the corresponding spinning frequency for the experimental parameters in Figs. 5–7, where the duration of a pulse sequence element is τ_C = 24.3 μs.

The plot shows that the $P = 2$ supercycle provides poor decoupling when $N = 4n$, i.e. when 4 decoupling cycles fit into 1 rotor period. This condition occurs at a spinning frequency close to 10 kHz for the chosen experimental parameters. In the case of the $P = 3$ supercycle, on the other hand, the conditions $N = 3n$ and $N = 6n$ should be avoided, while the $N = 4n$ condition is unproblematic. For the chosen experimental conditions in which the cycle duration is τ_C = 24.3 μs, good decoupling may therefore be achieved at spinning frequencies around 10 kHz by choosing the $P = 3$ supercycle instead of $P = 2$. At higher spinning frequencies, on the other hand, the $P = 2$ supercycle is better.

Fig. 8 shows that increasing the supercycle order beyond $P = 3$ at first leads to an increasing number of recoupling resonances, which is undesirable. However, the resonances thin out again for large values of *P*. This regime may be interesting to explore experimentally.

Fig. 8 indicates that the value $P = 1$, corresponding to the absence of a supercycle, leads to the lowest density of recoupling conditions. The advantages of supercycled decoupling sequences (improved robustness, improved spectral appearance, etc.) are therefore accompanied by the disadvantage of having to select the supercycle order according to the desired spinning frequency and RF field strength. The analysis given in this section allows this to be done in a straightforward and rigorous way.

5. Conclusions

We have introduced a supercycled version of *w*DUMBO, denoted by *w*DUMBO-S2, with an improved performance. We have compared *w*PMLG-S2 and *w*DUMBO-S2 schemes and observed that the performance efficiency of both are nearly the same except that *w*DUMBO-S2 requires a slightly higher RF power level than *w*PMLG-S2 for a given spinning speed. In all cases, rotary-resonance conditions occur at certain ratios of spinning frequency and cycle frequency and must be avoided if the best resolution is desired. It is possible to introduce different supercycling schemes, such as in *w*PMLG-S3, to obtain high-quality spectra under conditions for which the normal *w*PMLG-S2 supercycle provides relatively poor performance. The ^1H spectral resolution obtained with any of the homonuclear dipolar decoupling scheme discussed here is nearly the same under similar experimental conditions.

Acknowledgments

We thank the financial support by the Royal Society (UK) and the British Council of India, EPSRC (UK), the use of National Facility for High-Field NMR, TIFR, for the use of the Bruker AV500 spectrometer, and M.V. Naik for technical assistance.

References

[1] B.C. Gerstein, C. Clor, R.G. Pembelton, R.C. Wilson, Utility of pulse nuclear magnetic resonance in studying protons in coals, J. Phys. Chem. 81 (1977) 565.
[2] E. Vinogradov, P.K. Madhu, S. Vega, Strategies for high-resolution proton spectroscopy in solid-state NMR, Top. Curr. Chem. 246 (2005) 33.
[3] M. Mehring, J.S. Waugh, Magic-angle NMR experiments in solids, Phys. Rev. B5 (1972) 3459.
[4] M.H. Levitt, A. Bielecki, A.C. Kolbert, D.J. Ruben, Frequency-switched pulse sequences: homonuclear decoupling and dilute spin NMR in solids, Solid State NMR 2 (1993) 151.
[5] E. Vinogradov, P.K. Madhu, S. Vega, High-resolution proton solid-state NMR spectroscopy by phase-modulated Lee–Goldburg experiment, Chem. Phys. Lett. 314 (1999) 443.
[6] E. Vinogradov, P.K. Madhu, S. Vega, Phase modulated Lee–Goldburg magic angle spinning proton nuclear magnetic resonance experiments in the solid state: a bimodal Floquet theoretical treatment, J. Chem. Phys. 115 (2001) 8983.
[7] D. Sakellariou, A. Lesage, P. Hodgkinson, L. Emsley, Homonuclear dipolar decoupling in solid-state NMR using continuous phase modulation, Chem. Phys. Lett. 319 (2000) 253.
[8] J.J. Lopez, A.J. Mason, C. Kaiser, C. Glaubitz, Separated local field NMR experiments on oriented samples rotating at the magic angle, J. Biomol. NMR 37 (2007) 97.
[9] A.A. Nevzorov, S.J. Opella, Selective averaging for high-resolution solid-state NMR spectroscopy of aligned samples, J. Magn. Reson. 185 (2007) 59.
[10] R.G. Mavinkurve, H.S. Vinay Deepak, K.V. Ramanathan, N. Suryaprakash, Analyses of the complex proton NMR spectra: determination of anisotropic proton chemical shifts of oriented molecules by a two dimensional experiment, J. Magn. Reson. 185 (2007) 240.
[11] C.A. Steinbeck, M. Ernst, B.H. Meier, B.F. Chmelka, Anisotropic optical properties and structures of block copolymer/silica thin films containing aligned porphyrin J-aggregates, J. Phys. Chem. C112 (2008) 2565.
[12] E.R. deAzevedo, K. Saalwachter, O. Pascui, A.A. de Souza, T.J. Bonagamba, D. Reichert, Intermediate motions as studied by solid-state separated local field NMR experiments, J. Chem. Phys. 128 (2008) 104505.
[13] P.K. Madhu, E. Vinogradov, S. Vega, Multiple-pulse and magic-angle spinning aided double-quantum proton solid-state NMR spectroscopy, Chem. Phys. Lett. 394 (2004) 423.
[14] S.P. Brown, A. Lesage, B. Elena, L. Emsley, Probing proton–proton proximities in the solid state: high-resolution two-dimensional ^{1}H–^{1}H double-quantum CRAMPS NMR spectroscopy, J. Am. Chem. Soc. 126 (2004) 13230.
[15] B. Elena, G. Pintacuda, N. Mifsud, L. Emsley, Molecular structure determination in powders by NMR crystallography from proton spin diffusion, J. Am. Chem. Soc. 128 (2006) 9555.
[16] P. Avenier, A. Lesage, M. Taoufik, A. Baudouin, A. De Mallmann, S. Fiddy, M. Vautier, L. Veyre, J.M. Basset, L. Emsley, E.A. Quadrelli, Well-defined surface imido amido tantalum(V) species from ammonia and silica-supported tantalum hydrides, J. Am. Chem. Soc. 129 (2007) 176.
[17] C. Coelho, J. Rocha, P.K. Madhu, L. Mafra, Practical aspects of Lee–Goldburg based CRAMPS techniques for high-resolution ^{1}H NMR spectroscopy in solids, J. Magn. Reson. 194 (2008) 264.
[18] E. Vinogradov, P.K. Madhu, S. Vega, Proton spectroscopy in solid state nuclear magnetic resonance with windowed phase-modulated Lee–Goldburg decoupling sequences, Chem. Phys. Lett. 354 (2002) 193.
[19] M. Leskes, P.K. Madhu, S. Vega, A broad-banded z-rotation windowed phase-modulated Lee–Goldburg pulse sequence for ^{1}H spectroscopy in solid-state NMR, Chem. Phys. Lett. 447 (2007) 370.
[20] M. Leskes, P.K. Madhu, S. Vega, Supercycled homonuclear dipolar decoupling in solid-state NMR: toward cleaner ^{1}H spectrum and higher spinning rates, J. Chem. Phys. 128 (2008) 052309.
[21] A. Lesage, D. Sakellariou, S. Hedier, B. Elena, P. Charmont, S. Steuerngel, L. Emsley, Experimental aspects of proton NMR spectroscopy in solids using phase-modulated homonuclear dipolar decoupling, J. Magn. Reson. 163 (2003) 105.
[22] R. Keller, K. Wüthrich, Computer-aided resonance assignment (CARA), available from: <http://www.nmr.ch>.
[23] M. Hohwy, P.V. Bower, H.J. Jakobsen, N.C. Nielsen, A high-order and broadband CRAMPS experiment using z-rotational decoupling, Chem. Phys. Lett. 273 (1997) 297.
[24] M. Hohwy, N.C. Nielsen, Elimination of high order terms in multiple pulse nuclear magnetic resonance spectroscopy: application to homonuclear decoupling in solids, J. Chem. Phys. 106 (1997) 7571.
[25] U. Haeberlen, High resolution NMR in solids-selective averaging, Supplement 1, Adv. Magn. Reson, Academic Press, New York, 1976.
[26] M. Edén, M.H. Levitt, Pulse sequence symmetries in the NMR of spinning solids. application to heteronuclear decoupling, J. Chem. Phys. 111 (1999) 1511.
[27] A. Brinkmann, M. Edén, M.H. Levitt, Synchronous helical pulse sequences in magic-angle spinning NMR. Double quantum recoupling of multiple-spin systems, J. Chem. Phys. 112 (2000) 8539.
[28] A. Brinkmann, M.H. Levitt, Symmetry principles in the nuclear magnetic resonance of spinning solids: heteronuclear recoupling by generalized Hartmann–Hahn sequences, J. Chem. Phys. 115 (2001) 357.
[29] M.H. Levitt, Symmetry-based pulse sequences in magic-angle spinning solid-state NMR, in: D.M. Grant, R.K. Harris (Eds.), Encyclopedia of Nuclear Magnetic Resonance: Supplementary Volume, Wiley, Chichester, UK, 2002.
[30] M.H. Levitt, Symmetry in the design of NMR multiple-pulse sequences, J. Chem. Phys. 128 (2008) 52205.